Vectorial active matter on the lattice: emergence of polar condensates and nematic bands in an active zero-range process

Josué Manik Nava-Sedeño, Lutz Brusch, and Andreas Deutsch
Technische Universität Dresden, Center for Information Services and High Performance Computing, Nöthnitzer Straße 46, 01062 Dresden, Germany

Haralampos Hatzikirou
Department of Systems Immunology and Braunschweig Integrated Center of Systems Biology, Helmholtz Center for Infection Research, Inhoffenstraße 7, 38124 Braunschweig, Germany

Anja Voß-Böhme
Technische Universität Dresden, Center for Information Services and High Performance Computing, Nöthnitzer Straße 46, 01062 Dresden, Germany and Fakultät Informatik/Mathematik, Hochschule für Technik und Wirtschaft, Dresden, Germany.

Fernando Peruani
Université Côte d'Azur, Laboratoire J. A. Dieudonné, UMR 7351 CNRS, Parc Valrose, F-06108 Nice Cedex 02, France

Abstract

We introduce a lattice-gas cellular automaton (LGCA) for vectorial active matter, considering both, polar and nematic velocity alignment. Interactions are by construction zero-range. We show that above a critical density in the LGCA with polar alignment, a polar condensate emerges. In the LGCA with nematic alignment, the system self-organizes, above a critical density, in spatially elongated, high-density, nematic bands, despite de fact interaction are zero-range. In order to rationalize these findings, we derive the corresponding hydrodynamic equations of the proposed LGCA for vectorial active matter.

I. INTRODUCTION

Self-organized patterns of self-propelled entities are found at all scale in biology: from *in vitro* cytoskeletal extracts [1–3], bacterial systems [4–8], and insect swarms [9] to school of fish [10], herds of mammals [11], and human crowds [12]. Collective phenomena are also observed in artificial active systems such as synthetic swimmers [13, 14], phoretic colloids [15, 16], and active rollers [17–19]. Except for (neutral) phase separation [20], other complex, self-organized, collective motion patterns involve either polar or nematic (orientational) order. Given the vectorial nature of orientational order, active systems sharing such a feature are often referred to vectorial active matter. It is widely believed that self-organized patterns in vectorial active matter require particles to interact via some type of velocity alignement mechanism [21, 22]. The best known example of an active system with a polar velocity alignement is the Vicsek model [23], where complex, active polar flows spontaneously emerge. A different "universality class" of active systems is obtained by switching in the Vicsek model to a nematic velocity alignement [24, 25]. Self-propelled particles with nematic alignement do not form polar flows, but self-organize into high-density, nematic bands [25]. The theoretical understanding vectorial active matter is strongly based on the study of minimal, Vicsek-like models by means of numerically costly, particle-based simulations [23, 25–27] and by the derivation of hydrodynamic equations [28–32]; for comprehensive reviews, see [21, 22].

Here, we introduce a numerically efficient lattice-gas cellular automaton (LGCA) for vectorial active matter, considering both, polar and nematic velocity alignment. Interactions are by construction zero-range. We show that above a critical density the LGCA with polar alignment undergoes a phase transition from a disordered, dilute phase to a phase characterized by the presence of one or a reduced number polar, actively moving condensates that possess a macroscopic fraction of the number of particles in the system. In the LGCA with nematic alignment, the system self-organizes, above a critical density, in spatially elongated, high-density, nematic bands, despite de fact interaction are zero-range. We make use of the local nature of the interaction to derive the corresponding hydrodynamic equations of the proposed LGCA for vectorial active matter.

II. MODEL DEFINITION

Lattice-gas cellular automaton (LGCA) models are defined on a regular lattice $\mathcal{L} \subset \mathbb{R}^d$, whose coordination number, equal to the number of first neighbors, is given by b. Throught this work, it will be assumed that $d = 2$ and $b = 6$, a hexagonal lattice. The set of lattice angles is given by $\Theta = \left\{ \frac{2n\pi}{b} : n \in \mathbb{N}, 0 \leq n < b \right\}$. To each lattice site $\vec{r} \in \mathcal{L}$ are associated b velocity channels $\vec{c}_\vartheta \coloneqq (\cos\vartheta, \sin\vartheta)$, $\vartheta \in \Theta$. Each velocity channel can be occupied by $s_\vartheta \in \mathbb{N}$ particles which, together, determine the state of the lattice site $\vec{s}$. The state of the lattice evolves in discrete time steps by the subsequent application of a stochastic reorientation step followed by a deterministic transport step synchronously to all lattice sites. During the reorientation step, every individual particle is independently assigned a new velocity channel $\vec{c}_\theta$ with a probability $T_\vartheta(\vec{s})$ given the state of their lattice site. Here we will consider zero-range velocity alignment probabilities

$$T_\vartheta(\vec{s}) = \frac{1}{Z} \exp\left[\beta \sum_{\theta \in \Theta} s_\theta \left(\vec{c}_\vartheta \cdot \vec{c}_\theta \right)^m \right], \tag{1}$$

where $\beta \in \mathbb{R}_+$ is the sensitivity which determines the strength of the alignment, Z is the normalization constant, and $m = 1$ if the alignment is polar, while $m = 2$ if the alignment is nematic. The state of the node after reorientation is denoted by $\vec{s}^{\mathcal{I}}$. After all particles in all velocity channels in all lattice sites have been redistributed, during the transport step all particles are translocated to the same velocity channel in a neighboring node in the direction of their velocity channel, see Fig. 1 for a depiction of the dynamics of the LGCA. The dynamics of the lattice is therefore given by the microdynamical equation $s_\vartheta(\vec{r} + \vec{c}_\vartheta, k+1) = s^{\mathcal{I}}_\vartheta(\vec{r}, k)$.

III. MODEL CHARACTERIZATION

The model shows qualitatively different behavior, depending on the type of alignment (Fig. 2). Starting from the homogeneous, disordered state, for high enough densities and sensibilities, the polar alignment model shows the formation of single high density lattice sites (condensates) with all particles within them having the same velocities. Particle number distributions show identical condensation behavior as the classic zero range process (Evans and Hanney, 2005), with well defined and separate dilute and condensed phases. Under

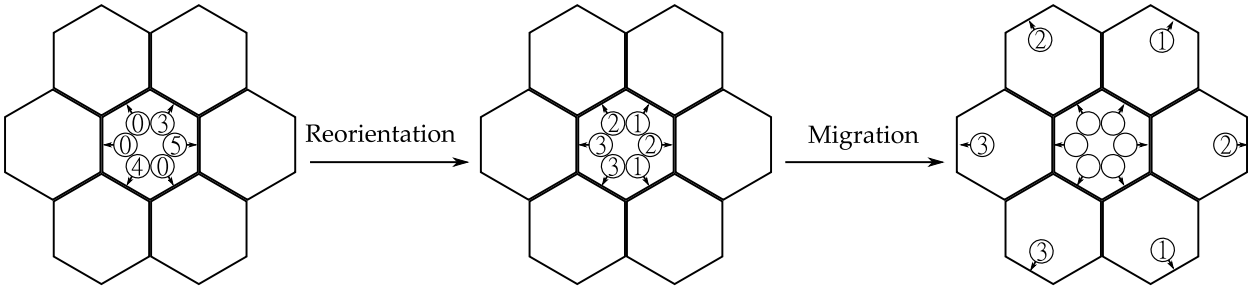

FIG. 1: LGCA dyamics. Particles reside in velocity channels within lattice sites. During the interaction step, particles within each lattice site are independently assigned new velocity channels according to the probability $T_\vartheta(\vec{s})$. After the interaction step, particles are deterministically moved to neighboring lattice sites during the migration step.

similar conditions, the model with nematic alignment shows the formation of long bands of lattice sites with high density and perfect nematic order. In this case, particle number distributions show a continuum between dilute and condensed phases. Furthermore, observables quantitatively show that band patterning occurs in the nematic case (as opposed to the polar case), in spite of the interaction not considering neighbor information. Computationally, the critical density and sensitivity were found by calculating the polar/nematic order parameter defined as $\Phi_m = \left\langle \left| \frac{1}{N} \sum_{k=1}^{N} e^{i\alpha\vartheta_k} \right| \right\rangle$, where N is the number of particles in the lattice, and m as defined previously. Analogous results are obtained by using clustring and band formation parameters. Doing a steady state stability analysis of the homogeneous, disordered state of the latice-Boltzmann equation, we find that the transition occurs much earlier than predicted by the theory (Fig. 2 solid line). If we take into account the fluctuations produced by the multinomial velocity reordering process, the transition is much better approximated (Fig. 2 dashed line).

IV. MACROSCOPIC PDES

The macroscopic dynamics of the model can be described in an approximate manner by calculating the expected value of velocity channel occupations from the microdynamical equation of the lattice. As a first step, the quantities $f_\vartheta(\vec{r},k) \coloneqq \langle s_\vartheta(\vec{r},k)\rangle$ are defined, which are the average number of particles moving in the direction defined by the lattice angle ϑ, and are proportional to the probability of particles in a node to move in that

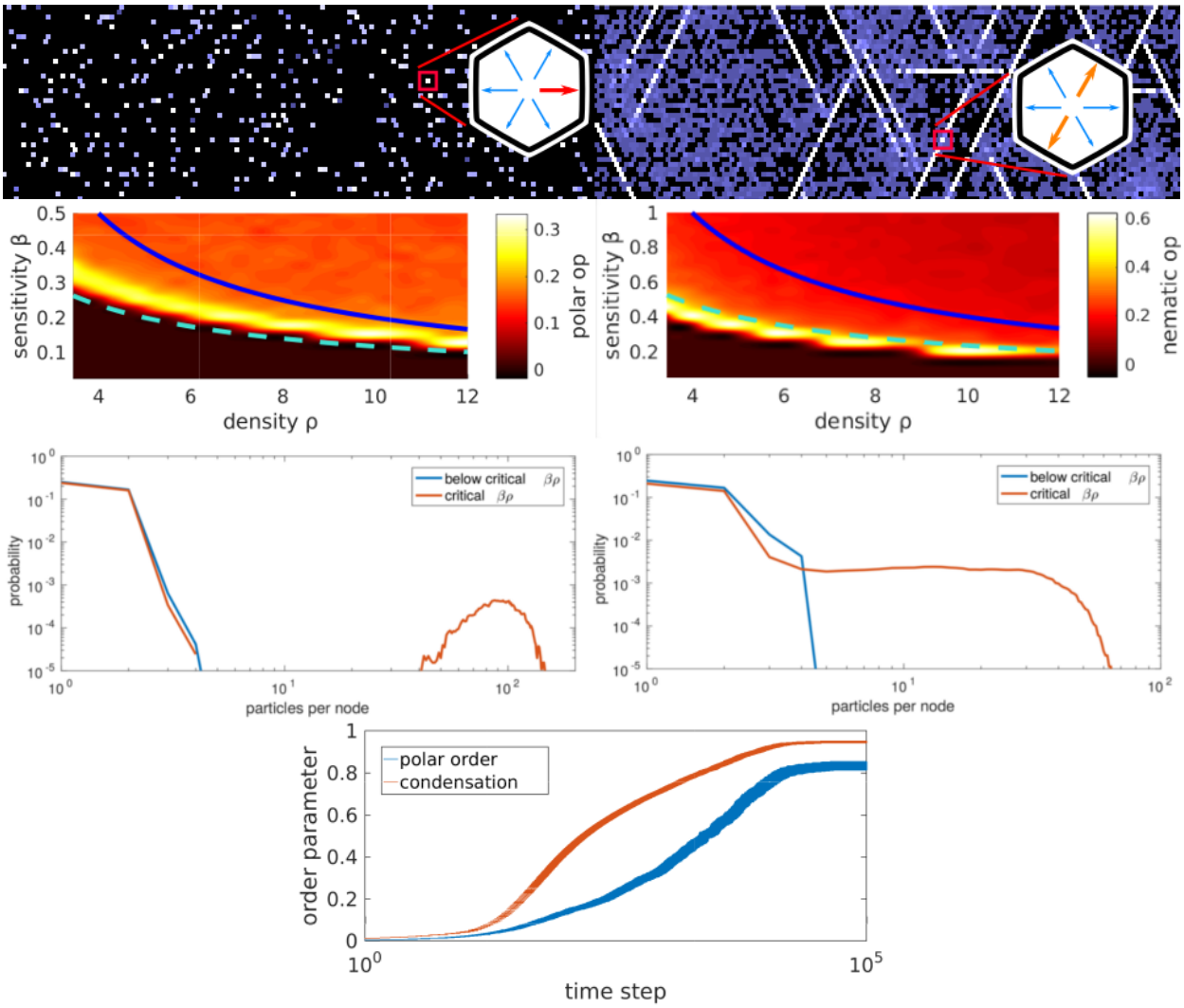

FIG. 2: Results from LGCA simulations. Polar (left) and nematic (right) alignment. Snapshots of simulations after 1000 time steps (top row). Empty lattice sites are shown in black. Occupied lattice sites appear whiter the higher the number of particles in them. The initial condition was the homogeneous, disordered state with exactly one particle in every velocity channel ($n = 6$). The sensitivity was fixed at $\beta = 0.3$. In both systems, the steady state has not been reached, but the condensation process can be visualized. Polar and nematic order parameters obtained from simulations at different values of the sensitivity and mean density (second row from top). Colors correspond to the value of the corresponding order parameter. Solid lines correspond to the critical parameters according to the linear stability analysis, while dashed lines represent these corrected to account for density fluctuations. Simulations were performed on a 60×60 lattice with disordered homogeneous initial conditions for 1000 time steps with varying β and ρ. The observables were averaged over 200 simulations. Probability of finding an occupied lattice site with a certain number of particles for zero-range velocity alignment models (second row from bottom). Two parameter combinations were sumulated: before the onset (blue line, $\beta = 1$ and $\rho = 0.12$ for polar, $\beta = 1$ and $\rho = 0.72$ for nematic alignment), and at the onset of condensation (red line, $\beta = 1$ and $\rho = 0.6$ for polar, $\beta = 1$ and $\rho = 1.2$ for nematic alignment). Mean polar order parameter and condensed

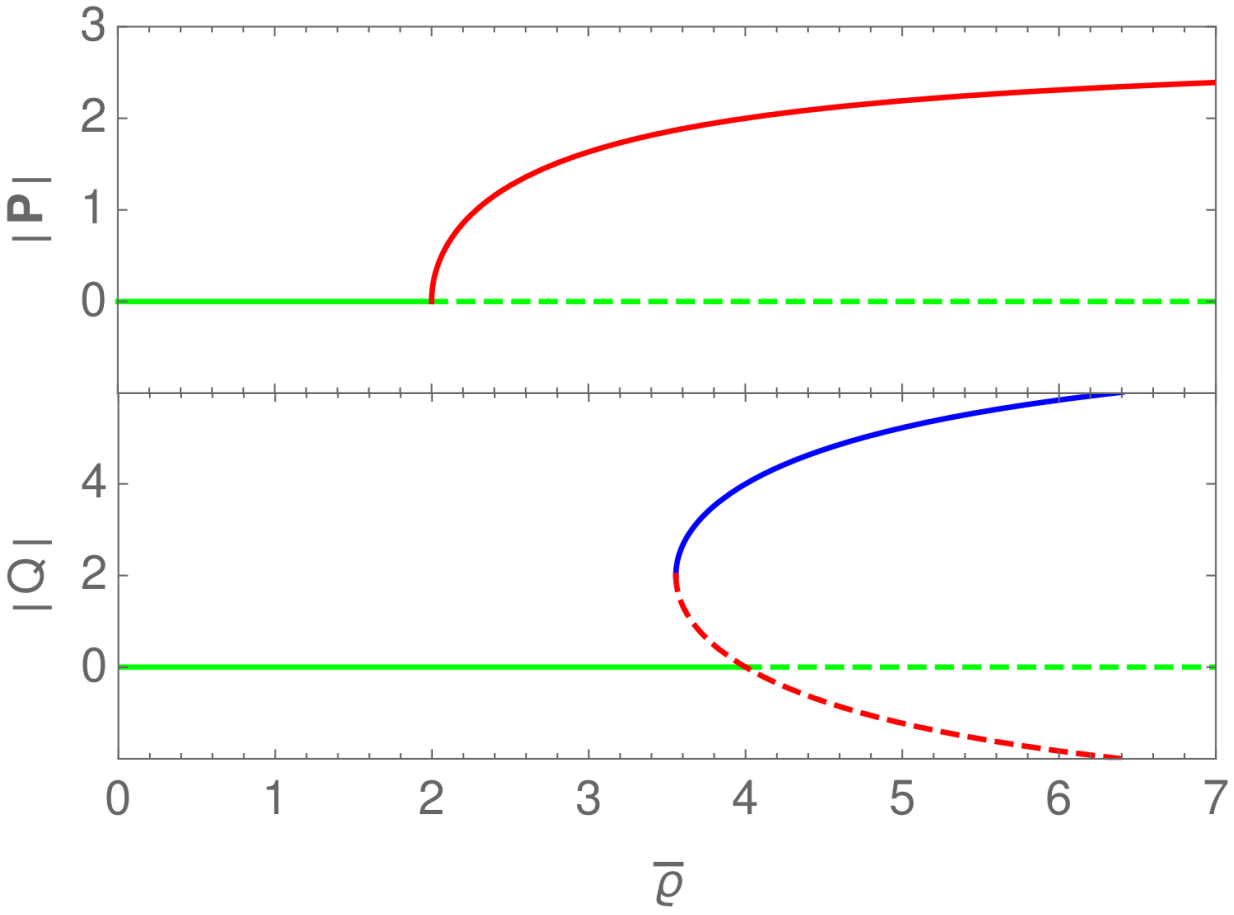

FIG. 3: Homogeneous steady states of the macroscopic PDE approximations. Polar (top) and nematic (bottom) alignment. Uniformly stable steady states are shown with solid lines, while uniformly unstable steady states are shown with dashed lines. Colors are used to distinguish different steady state solutions.

direction. Calculating the expectations from the microdynamical equation, a deterministic lattice-Boltzmann equation can be obtained by performing an in-node mean-field approximation and employing the binomial statistics of velocity channel occupation, yielding $f_\vartheta\left(\vec{r}+\vec{c}_\vartheta, k+1\right) = n\left(\vec{r},k\right) T_\vartheta\left(\vec{r},k\right)$, where $n\left(\vec{r},k\right) \coloneqq \sum_{\vartheta\in\Theta} f_\vartheta\left(\vec{r},k\right)$ is the density, or expected number of particles in a lattice site, and $T_\vartheta\left(\vec{r},k\right) \coloneqq \frac{1}{Z}\exp\left[\beta \sum_{\theta\in\Theta} f_\theta\left(\vec{r},k\right)\left(\vec{c}_\vartheta\cdot\vec{c}_\theta\right)^m\right]$ is the mean-field alignment probability. Discrete space and time are scaled to continuous space and time through defining a lattice spacing ε and a time step length τ. Differential equations are approximated from the difference LBE, by letting $\varepsilon,\tau\to 0$. As the continuous LBE is still dependent on the microscopic lattice angles ϑ, a discrete Fourier trans-

form is performed on the differential LBE. This results in differential equations for each of the discrete Fourier coefficients, which are related to macroscopic quantities. In contrast to similar derivations starting from continuous agent-based models, the number of Fourier coefficients is finite and equal to the number of lattice angles, and thus dependent on the lattice geometry. In the case of a hexagonal lattice (which is assumed throughout this work), the macroscopic quantities, defined through the discrete Fourier coefficients, are density $\rho\left(\vec{x},t\right) \coloneqq \sum_{\vartheta\in\Theta} f_\vartheta\left(\vec{x},t\right)$, momentum $\vec{P}\left(\vec{x},t\right) \coloneqq \left(\sum_{\vartheta\in\Theta} f_\vartheta\left(\vec{x},t\right)\cos\vartheta, \sum_{\vartheta\in\Theta} f_\vartheta\left(\vec{x},t\right)\sin\vartheta\right)$, and nematic anisotropy $Q\left(\vec{x},t\right) \coloneqq \sum_{\vartheta\in\Theta} f_\vartheta\left(\vec{x},t\right)\cos 2\vartheta + i\sum_{\vartheta\in\Theta} f_\vartheta\left(\vec{x},t\right)\sin 2\vartheta$. The last Fourier coefficient was unused.

A. Zero-range polar alignment

For polar alignment, the set of six PDEs for each Fourier coefficient was reduced to two, namely, a scalar equation for the density, and a vectorial equation for the momentum. The reduction was achieved by considering the system to be near the ordered state. The resulting PDEs read

$$\partial_t \varrho + \nabla\cdot\vec{P} = 0 \tag{2a}$$

$$\begin{aligned}\partial_t\vec{P} + \frac{1}{2}\left[\nabla\varrho - \mathcal{D}\left(\nabla\varrho\right)\right] + \\ \frac{1}{\varrho}\left[\left(\vec{P}\cdot\nabla\right)\vec{P} - \frac{1}{2}\nabla P^2 + \left(\nabla\cdot\vec{P}\right)\vec{P}\right] \\ = \vec{P}\left[\frac{\varrho}{2}\left(1-\frac{P^2}{8}\right) - 1\right],\end{aligned} \tag{2b}$$

where ϱ is the nondimensional density, $\vec{P}$ is the nondimensional momentum, and the operator $\mathcal{D}\left(\nabla\varrho\right) \coloneqq \frac{1}{\varrho^2}\left[\vec{P}\left(\vec{P}\cdot\nabla\varrho\right) + \left\|\vec{P}\times\left(\vec{P}\times\nabla\varrho\right)\right\|\right]$.

We find two spatially homogeneous steady states with $\varrho = \bar{\varrho}$ equal to an arbitrary positive constant. The first steady state is the disordered homogeneous steady state with $\vec{P} = \vec{0}$. Performing a linear stability analysis around this steady state, and assuming perturbations along a single direction, we find a density eigenvalue, and two momentum eigenvalues. The momentum eigenvalues indicate that the system is stable against uniform perturbations for $\bar{\varrho} < 2$ (Fig. 3). This is the same stability condition found when performing the stability analysis of the original lattice-gas model. The full eigenvalue spectrum of the disordered state is qualitatively similar to that found by Bussemaker *et al.* (1997) for a system of polar

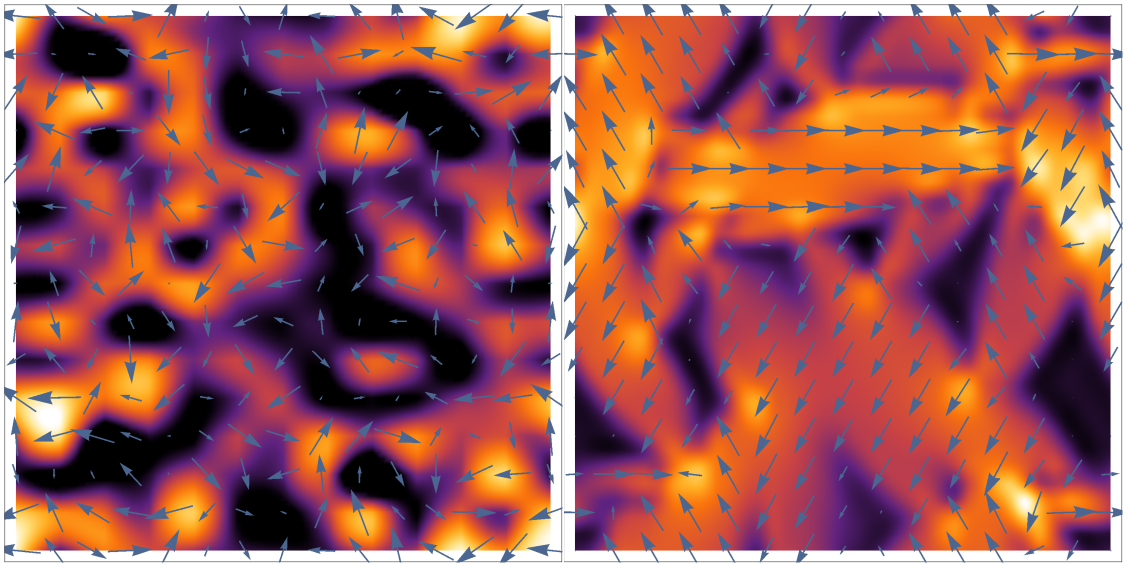

FIG. 4: Numeric evaluation of the PDE approximations. Polar (top) and nematic (bottom) alignment. Colors represent the value of the non-dimensional density ϱ, while the vector field is a representation of the momentum $\vec{P}$ and nematic anisotropy Q, for the polar and nematic case, respectively. The system was initialized at the homogenenous isotropic steady state with $\bar{\varrho} = 4$ (polar) and $\bar{\varrho} = 8$ (nematic), plus random splines of 0.2 amplitude. The snapshot was taken at $t = 1000$. Periodic boundary conditions were used.

aligning particles with an extended neighborhood of interaction and an exclusion principle among particles.

The second steady state is an anisotropic state with spatially homogeneous momentum $\vec{P} = \sqrt{8\left(1 - \frac{2}{\bar{\varrho}}\right)}\,(\cos\phi, \sin\phi)$ where $\phi \in [0, 2\pi)$ is an arbitrary angle. The angle ϕ is not constrained by the lattice, as no lattice properties were used during the derivation of the PDEs. This state only exists when $\bar{\varrho} > 2$, where the disordered state becomes unstable (Fig. 3). We find a momentum eigenvalue, an eigenvalue corresponding to the normal to the momentum, and a mixed density-momentum eigenvalue. We consider the extreme cases $\phi = 0$ and $\phi = \frac{\pi}{2}$. The system is always stable against uniform perturbations. However, considering both extreme cases, for all non-uniform perturbations (wavenumber $q \neq 0$) the homogenenous anisotropic steady state is stable only for the parameter range $2.564 \lessapprox \bar{\varrho} < 3$. The real parts of the eigenvalues grow with increasing wavenumber, so we expect the homogeneous solution to break apart into small wavelength patterns. Numerical approximations to the PDE solutions confirm the stability condition found theoretically, and

show the formation of small aggregates, especially for high values of $\bar{\varrho}$, similar to the ones observed in the lattice-gas model (Fig. 4).

B. Zero-range nematic alignment

We also derived macroscopic equations for nematic alignment ($m = 2$). In this case, the equations were reduced to two, one for the density and one for the nematic anisotropy. This was achieved by assuming other macroscopic quantities reached the steady state much faster. The equations are lattice dependent and are different depending on the lattice geometry. For a hexagonal lattice, the macroscopic PDEs are

$$\partial_t \varrho = \mathfrak{d}\bar{\mathfrak{d}}\varrho + \mathfrak{R}\left(\mathfrak{d}^2\bar{Q}\right) \tag{3a}$$

$$\begin{aligned}\partial_t Q = &\frac{1}{2}\left\{\mathfrak{d}^2\varrho + \mathfrak{d}\bar{\mathfrak{d}}Q + 2\bar{\mathfrak{d}}\left[\mathfrak{R}\left(\mathfrak{d}Q\right)\right]\right\} \\ &+\frac{\varrho}{4}\left[Q + \frac{1}{8}\bar{Q}\left(\bar{Q} - \frac{1}{4}Q^2\right)\right] - Q,\end{aligned} \tag{3b}$$

where $Q \in \mathbb{C}$ is the dimensionless nematic anisotropy, $\mathfrak{d} \coloneqq \partial_x + i\partial_y$ is the Wirtinger derivative, $\bar{\cdot}$ represents the complex conjugate, and $\mathfrak{R}\left(\cdot\right)$ represents the real part.

In this case, there is also disordered and anisotropic homoeneous steady state solutions, with constant dimensionless density $\bar{\varrho}$. Performing a linear stability analysis around the disordered state ($Q = 0$), we find a density and two nematic eigenvalues. The eigenvalues indicate that the disordered state is stable when $\bar{\varrho} < 4$, which agrees with the stability condition found for the lattice-gas model.

Additionally, there a a family of anisotropic, homogenenous steady states, whose dimensionless nematic anisotropy is given by $Q = \left(2 \pm 2\sqrt{9 - \frac{32}{\bar{\varrho}}}\right) e^{i\frac{2k\pi}{3}}$, $k \in \{0, 1, 2\}$. From the equation of Q in the anisotropic steady state, two features ae noteworty. First, the anisotropic steady state exists when $\bar{\varrho} > \frac{32}{9}$, meaning it exists even in a certain parameter regime where the disordered state is stable. Second, while for $\frac{32}{9} < \bar{\varrho} < 4$ pairs of solutions with different moduli but same argument $\arg\left(Q\right) \in \left\{\frac{2k\pi}{3}, k \in \mathbb{N}\right\} \subset \Theta$ exist, for the parameter regime $\bar{\varrho} > 4$, six different solutions exist, each one with a different argument corresponding to one of the lattice directions $\vartheta \in \Theta$. The correspondence between the arguments of the anisotropic steady state solutions and the lattice directions stems from the fact that the lattice symmetries were used to close the system of macroscopic PDEs during derivation. Performing a linear stability analysis around these steady states, we find that

the solutions with the greatest moduli are stable for all wavenumbers, while the ones with the smallest moduli are always unstable. Interestingly, for the parameter regime $\bar{\varrho} > 4$ this means that the solutions with $\arg(Q) = \frac{2k\pi}{3}$ are stable, while those with $\arg(Q) = \frac{(2k+1)\pi}{3}$ are unstable. This is due to geometrical constraints on imposed on Q by the lattice. The effects of the underlying lattice can be observed in the solutions of the PDEs at long times and high enough nondimensional densities (Fig. 4).

V. DISCUSSION

In this paper, we constructed a novel extension of the traditional LGCA methodology, which disregards any kind of exclusion among particles in the model and, accoringly, named boson lattice-gas cellular automata, or BLGA. Using this extension, we defined a model of zero-range polar and nematic velocity-aligning particles. This model allows us to investigate both alignment and condensation phenomena in the same model, and facilitates the derivation of macroscopic PDE approximations by disregarding long-range neighbor interactions. We find that density fulctuations play an important role in destabilizing the disordered steady state. Importantly, we find that, while zero-range polar alignment results in classic condensation, zero-range nematic alignment results in a continuous spectrum of dilute-condensed phases, and produces spatially extended patterns. That extended spatial patterns occur even for a zero-range interaction shows that particle movement plays an important role in pattern formation as a mechanism of spatial spread of information.

The mcroscopic PDEs approximating the BLGA model of polar alignment show that both disordered and ordered steady states are unstable, the last one showing growth of small wavelength perturbations, also observed in the original BLGA model. The PDE approximation also shows a small parameter regime of stability of the homogeneous ordered state, not observed in the BLGA model. This is probably due to the the smoothness of solutions in the PDE approximation, in contrast with the independent behavior of lattice sites in the BLGA model.

Six ordered steady states are found for the nematic PDE approximation, where each solution has a nematic director parallel to one of the lattice directions. The stable steady states have nematic directors corresponding to particles perfectly along one of the three lattice axes in the BLGA model. Although the homogeneous, ordered steady states are

always stable for big enough nondimensional densities in the macorscopic models, there is slight condensation in the original BLGA models. This phenomenon is probably not observable in the PDE model due to their coarse-grained resolution.

The BLGA model constructed here considers no exclusion between particles and complete independence of between particles. Of course, in most applications, especially in biology, individuals experiment steric effects. For such applications the BLGA methodology must be etended to discourage individuals going in the direction of steeply increasing density gradient.

In this paper, we have derived macroscopic PDE approximations of microscopic BLGA models of zero-range velocity alignment. Although the effects of interactions with particles within an extended neihgborhood remain to be investigated, we have shown the potential of BLGA models for generating macroscopic PDE models describing the dynamics of systems of migrating, interacting particles at the population level.

---

[1] V. Schaller, C. Weber, C. Semmrich, E. Frey, and A. R. Bausch, Nature **467**, 73 (2010), ISSN 0028-0836, URL http://dx.doi.org/10.1038/nature09312.

[2] T. Sanchez, D. T. Chen, S. J. DeCamp, M. Heymann, and Z. Dogic, Nature **491**, 431 (2012).

[3] K. H. Nagai, Y. Sumino, R. Montagne, I. S. Aranson, and H. Chaté, Phys. Rev. Lett. **114**, 168001 (2015), URL http://link.aps.org/doi/10.1103/PhysRevLett.114.168001.

[4] C. Dombrowski, L. Cisneros, S. Chatkaew, R. E. Goldstein, and J. O. Kessler, Phys. Rev. Lett. **93**, 098103 (2004), URL https://link.aps.org/doi/10.1103/PhysRevLett.93.098103.

[5] A. Sokolov, I. S. Aranson, J. O. Kessler, and R. E. Goldstein, Phys. Rev. Lett. **98**, 158102 (2007), URL http://link.aps.org/abstract/PRL/v98/e158102.

[6] F. Peruani, J. Starruß, V. Jakovljevic, L. Søgaard-Andersen, A. Deutsch, and M. Bär, Phys. Rev. Lett. **108**, 098102 (2012), URL http://link.aps.org/doi/10.1103/PhysRevLett.108.098102.

[7] G. Ariel, A. Rabani, S. Benisty, J. D. Partridge, R. M. Harshey, and A. Beer, Nat. Commun. **6**, 8396 (2015).

[8] A. Beer and G. Ariel, Mov. Ecol. **7**, 9 (2019), ISSN 2051-3933, URL https://doi.org/10.1186/s40462-019-0153-9.

[9] A. Attanasi, A. Cavagna, L. Del Castello, I. Giardina, S. Melillo, L. Parisi, O. Pohl, B. Rossaro, E. Shen, E. Silvestri, et al., Phys. Rev. Lett. **113**, 238102 (2014), URL http://link.aps.org/doi/10.1103/PhysRevLett.113.238102.

[10] A. J. W. Ward, D. J. T. Sumpter, I. D. Couzin, P. J. B. Hart, and J. Krause, P. Natl. Acad. Sci. USA **105**, 6948 (2008), ISSN 0027-8424, URL http://www.pnas.org/content/105/19/6948.

[11] F. Ginelli, F. Peruani, M.-H. Pillot, H. Chaté, G. Theraulaz, and R. Bon, P. Natl. Acad. Sci. USA **112**, 12729 (2015), URL http://www.pnas.org/content/112/41/12729.abstract.

[12] M. Moussaïd, D. Helbing, and G. Theraulaz, P. Natl. Acad. Sci. USA **108**, 6884 (2011), URL http://www.pnas.org/content/108/17/6884.abstract.

[13] J. Palacci, S. Sacanna, A. P. Steinberg, D. J. Pine, and P. M. Chaikin, Science **339**, 936 (2013), URL http://www.sciencemag.org/content/339/6122/936.abstract.

[14] I. Theurkauff, C. Cottin-Bizonne, J. Palacci, C. Ybert, and L. Bocquet, Phys. Rev. Lett. **108**, 268303 (2012), URL http://link.aps.org/doi/10.1103/PhysRevLett.108.268303.

[15] I. Buttinoni, J. Bialké, F. Kümmel, H. Löwen, C. Bechinger, and T. Speck, Phys. Rev. Lett. **110**, 238301 (2013), URL http://link.aps.org/doi/10.1103/PhysRevLett.110.238301.

[16] R. Golestanian, T. B. Liverpool, and A. Ajdari, New J. Phys. **9**, 126 (2007), URL http://stacks.iop.org/1367-2630/9/i=5/a=126.

[17] A. Bricard, J.-B. Caussin, N. Desreumaux, O. Dauchot, and D. Bartolo, Nature **503**, 95 (2013).

[18] A. Bricard, J.-B. Caussin, D. Das, C. Savoie, V. Chikkadi, K. Shitara, O. Chepizhko, F. Peruani, D. Saintillan, and D. Bartolo, Nat. Commun. **6** (2015).

[19] A. Kaiser, A. Snezhko, and I. S. Aranson, Science Advances **3** (2017).

[20] L. Barberis and F. Peruani, J. Chem. Phys. **150**, 144905 (2019).

[21] T. Vicsek and A. Zafeiris, Phys. Rep. **517**, 71 (2012), URL http://www.sciencedirect.com/science/article/pii/S0370157312000968.

[22] M. Marchetti, J. Joanny, S. Ramaswamy, T. Liverpool, J. Prost, M. Rao, and R. Simha, Rev. Mod. Phys. **85**, 1143 (2013), URL http://link.aps.org/doi/10.1103/RevModPhys.85.1143.

[23] T. Vicsek, A. Czirók, E. Ben-Jacob, I. Cohen, and O. Shochet, Phys. Rev. Lett. **75**, 1226 (1995), URL http://link.aps.org/doi/10.1103/PhysRevLett.75.1226.

[24] F. Peruani, A. Deutsch, and M. Bär, Eur. Phys. J.: Spec. Top. **157**, 111 (2008), URL http:

//dx.doi.org/10.1140/epjst/e2008-00634-x.

[25] F. Ginelli, F. Peruani, M. Bär, and H. Chaté, Phys. Rev. Lett. **104**, 184502 (2010), URL http://link.aps.org/doi/10.1103/PhysRevLett.104.184502.

[26] H. Chaté, F. Ginelli, and R. Montagne, Phys. Rev. Lett. **96**, 180602 (2006), URL http://link.aps.org/doi/10.1103/PhysRevLett.96.180602.

[27] H. Chaté, F. Ginelli, G. Grégoire, F. Peruani, and F. Raynaud, Eur. Phys. J. B **64**, 451 (2008), ISSN 1434-6028, URL http://www.springerlink.com/content/391193p527q40773/.

[28] J. Toner and Y. Tu, Phys. Rev. Lett. **75**, 4326 (1995), URL http://link.aps.org/doi/10.1103/PhysRevLett.75.4326.

[29] E. Bertin, M. Droz, and G. Grégoire, Phys. Rev. E **74**, 022101 (2006), URL http://link.aps.org/doi/10.1103/PhysRevE.74.022101.

[30] T. Ihle, Phys. Rev. E **83**, 030901 (2011), URL http://link.aps.org/doi/10.1103/PhysRevE.83.030901.

[31] A. Peshkov, I. S. Aranson, E. Bertin, H. Chaté, and F. Ginelli, Phys. Rev. Lett. **109**, 268701 (2012), URL http://link.aps.org/doi/10.1103/PhysRevLett.109.268701.

[32] A. Peshkov, E. Bertin, F. Ginelli, and H. Chaté, Eur. Phys. J.: Spec. Top. **223**, 1315 (2014), ISSN 1951-6401, URL http://dx.doi.org/10.1140/epjst/e2014-02193-y.